Developmental Cell, Volume *26*

Supplemental Information

Wnt5a Directs Polarized Calcium Gradients by Recruiting Cortical Endoplasmic Reticulum to the Cell Trailing Edge

Eric S. Witze, Mary Katherine Connacher, Stephane Houel, Michael P. Schwartz, Mary K. Morphew, Leah Reid, David B. Sacks, Kristi S. Anseth, and Natalie G. Ahn

Inventory of Supplementary Materials:

A. SUPPLEMENTAL FIGURES

Figure S1. The WRAMP structure in HUVEC and C2C12 cells, related to Figure 1. WRAMP structures in **(A)** WM239a melanoma cells and **(B)** HUVEC cells. **(C)** Live cell images of HUVEC and C2C12 cells expressing MCAM-GFP reveal asymmetric polarization of MCAM immediately followed by membrane retraction. Thus, formation of the WRAMP structure is a general cellular event, not limited to melanoma cells.

Figure S2. Components of the WRAMP proteome, related to Figure 3. Spectral counts of identified proteins, quantified *vs* fraction number (with highest density in fr #1), in cells treated with (●) or without (○) Wnt5a. Indicated are proteins that showed increased abundance in fr #2 in response to Wnt5a, in addition to those presented in **Fig. 3**. **(A-F)** Cytoskeletal proteins dynein 1 heavy chain (DYNC1H1), gelsolin (GSN), myosin IIa (MYH9), myosin 1b (MYO1B), nuclear distribution gene C (NUDC), and tubulin α1b (TUBA1B). **(G-J)** Protein binding and recognition proteins TCP1 subunit 5 chaperone protein (CCT5), exportin 2 (CSE1L), karyopherin (importin) β1 (KPNB1), and poly rC binding protein 1 (PCBP1). **(K,L,O)** Membrane trafficking proteins coatomers , COP-Iα (COPA), COP-Iγ (COPG), and COP-Iδ (COPD). **(M,N,P-R)** Proteins with enzymatic function: calpain-2 (CAPN2), p21-activated kinase-2 (PAK2), PP2A regulatory subunit A-α (PPP2R1A), fatty acid synthase (FASN), and ribonuclease inhibitor-1 (RNH1). For details see the full table in **Suppl. Table S1**.

Figure S3. Calcium elevation at the WRAMP structure, related to Figure 7. (A) ER-RFP (top panels) and Cameleon (bottom panels) signals at indicated times after Wnt5a addition. Arrows point to the WRAMP structure. (B) Quantification of free calcium within the WRAMP structure (green) and within a separate region outside of the WRAMP structure (blue) at varying times after Wnt5a addition.

Figure S1

A WM239A melanoma cells

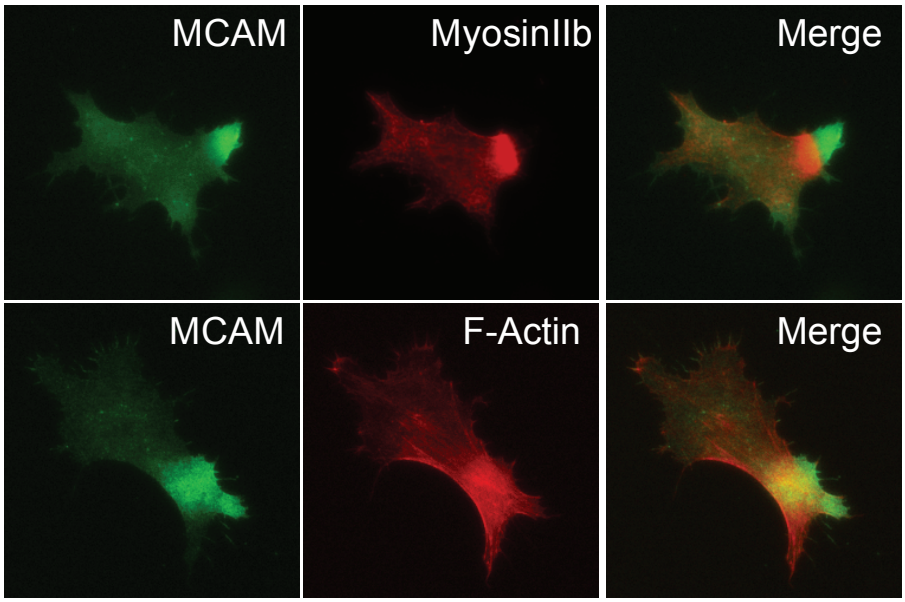

B Human vascular endothelial cells (HUVEC)

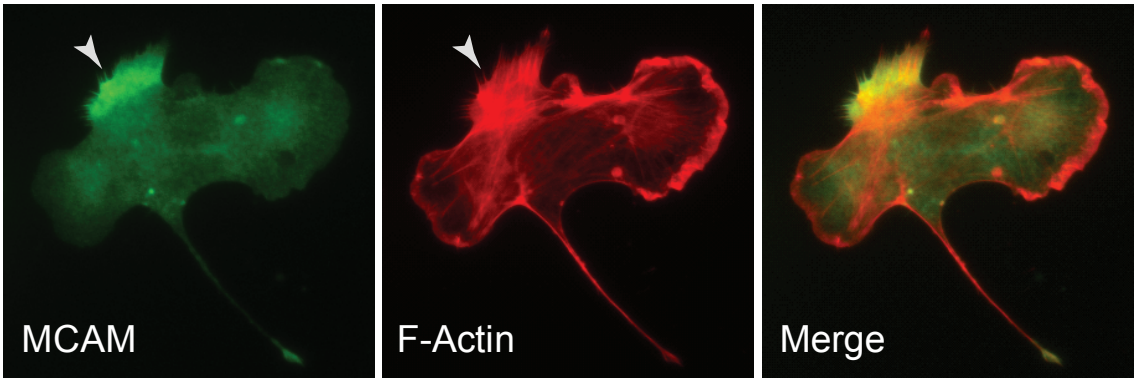

C C2C12 myoblast cells HUVEC cells

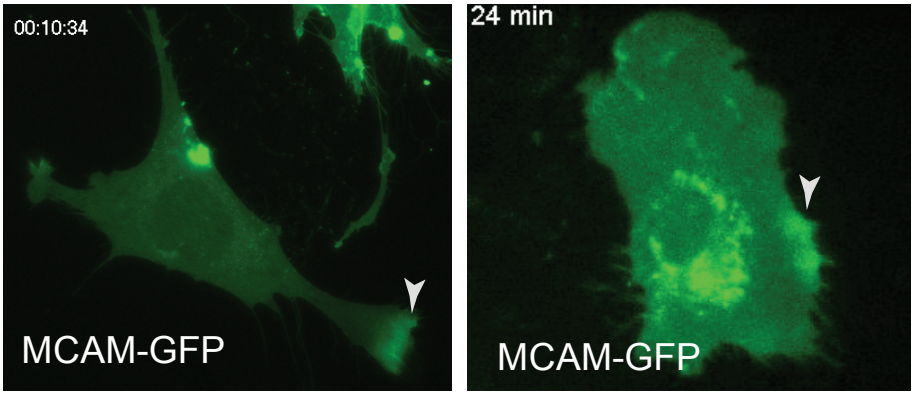

Figure S2

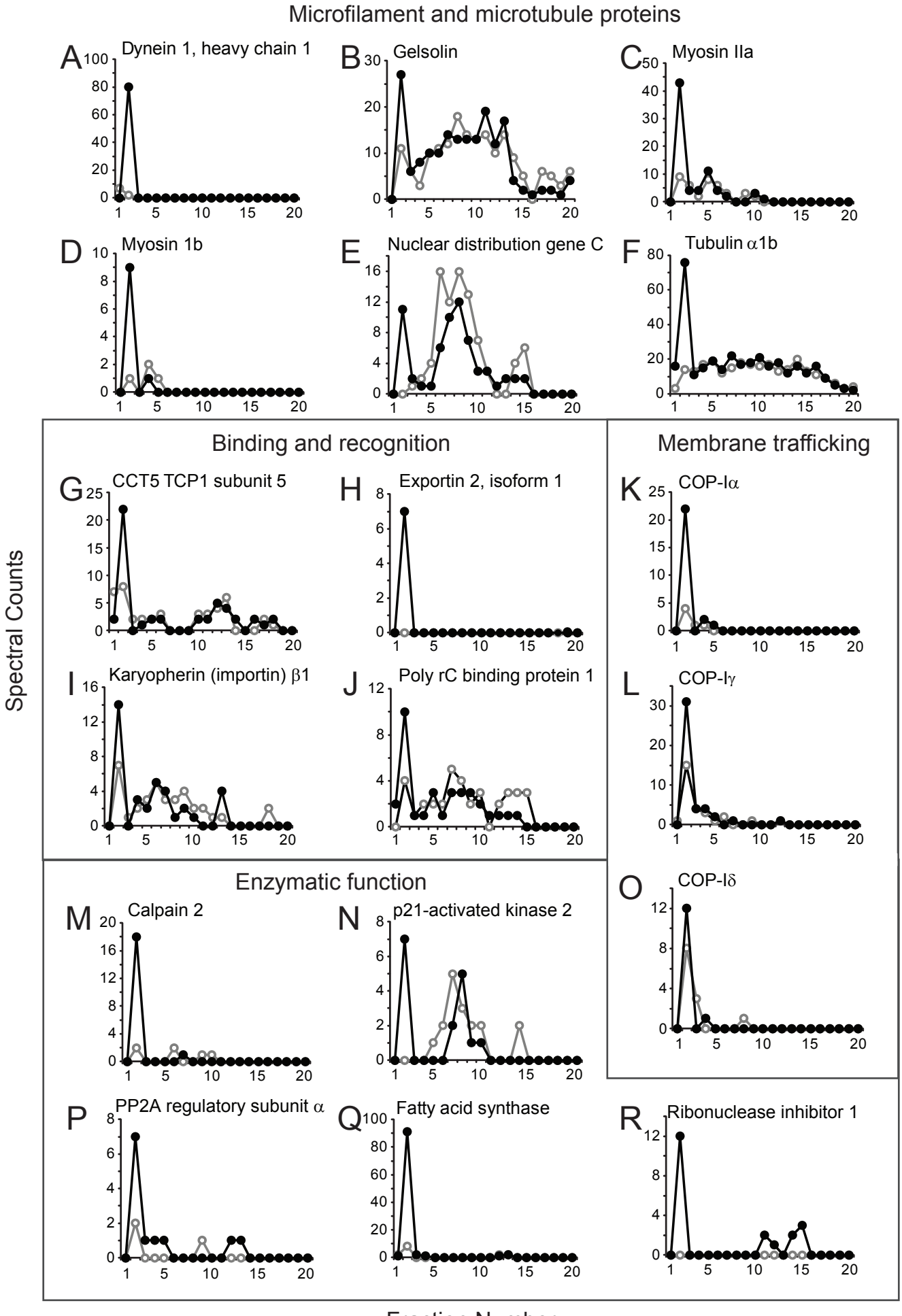
Microfilament and microtubule proteins
A
Dynein 1, heavy chain 1
B
Gelsolin
C
Myosin IIa
D
Myosin 1b
E
Nuclear distribution gene C
F
Tubulin α1b
Binding and recognition
G
CCT5 TCP1 subunit 5
H
Exportin 2, isoform 1
I
Karyopherin (importin) β1
J
Poly rC binding protein 1
Membrane trafficking
K
COP-Iα
L
COP-Iγ
O
COP-Iδ
Enzymatic function
M
Calpain 2
N
p21-activated kinase 2
P
PP2A regulatory subunit α
Q
Fatty acid synthase
R
Ribonuclease inhibitor 1
Spectral Counts
Fraction Number

Figure S3

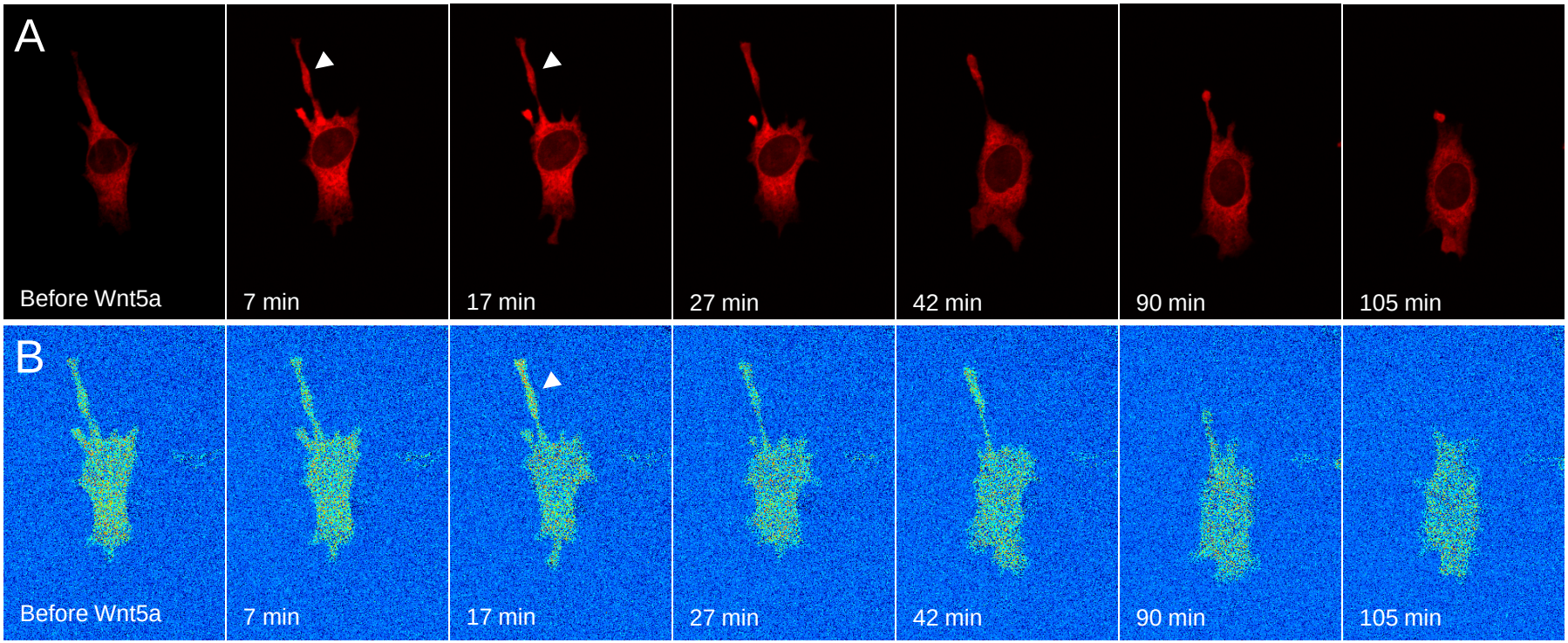
A
Before Wnt5a
7 min
17 min
27 min
42 min
90 min
105 min
B
Before Wnt5a
7 min
17 min
27 min
42 min
90 min
105 min

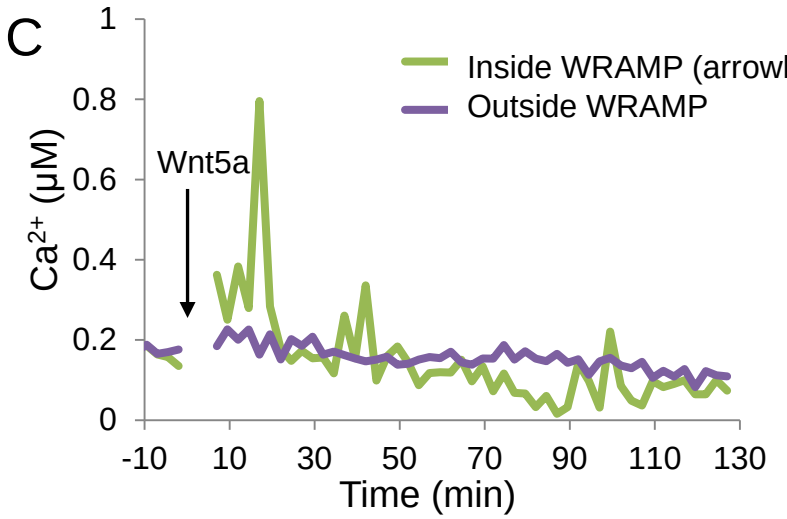
C
Inside WRAMP (arrowhead)
Outside WRAMP
Wnt5a
Ca2+ (µM)
1
0.8
0.6
0.4
0.2
0
-10
10
30
50
70
90
110
130
Time (min)

B. SUPPLEMENTAL TABLES

Table S1. Proteins in all LC-MS/MS datasets, related to Figure 2.
See separate Excel File: "Witze et al_Table S1_Proteins in all LCMSMS datasets.xls"

Table S2. Components of the WRAMP proteome, related to Figure 3.

Table S2. Components of the WRAMP proteome

Gene Symbol	Protein Name (UniProtKB)	Function	Fraction #2 Spectral Counts		Total Spectral Counts	
			Control	Wnt5a	Control	Wnt5a
Actin dynamics						
FLNA	Filamin-A (P21333)	Actin organization, microfilament linkage to cell membranes, integrin activation and recycling, cell adhesion and movement (1)	15	44	109	125
GSN	Gelsolin (P06396)	Ca2+ and PIP2 dependent actin capping and severing activity (2)	11	27	170	178
IQGAP1	IQ motif containing GTPase activating protein 1 (P46940)	Binds calmodulin, regulates actin assembly and cell motility, MAP kinase scaffold (3)	5	20	82	111
MYH9	Nonmuscle myosin heavy chain IIA (P35579)	Actin based movement, cytokinesis, cell shape and motility (4)	9	43	39	72
MYO1B	Myosin 1B (O43795)	Actin motor similarity, six IQ domains. Implicated in cell migration, neurite outgrowth, vesicle transport (5)	1	9	4	10
TLN1	Talin-1 (Q9Y490)	Actin filament anchoring at the plasma membrane, cell attachment and migration (6)	16	87	110	171
Microtubule dynamics						
DYNC1H1	Dynein heavy chain 1 (Q14204)	Microtubule motor, organelle movement, protein sorting, spindle dynamics (7)	2	80	9	80
NUDC	Nuclear migration protein nudC (Q9Y266)	Chaperone which mediates interaction of kinesin-1 with dynein and dynactin, and axon anterograde transport (8)	0	11	84	63
TUBA1B	Tubulin, alpha-IB (P68363)	Microtubule polymerization (9)	14	76	254	338
Cell adhesion and movement						
FAM129B/ Minerva	Protein family 129, member B/ Melanoma ERK-dependent invasion (Q96TA1)	Cancer cell invasion via phosphorylation by MAP kinase (10)	3	17	28	62
FERMT3	Fermitin family member 3/ Kindlin (Q86UX7)	Protein interactions for integrin activation and cell adhesion (11)	4	15	35	50
Membrane trafficking						
CLTCL1	Clathrin heavy chain like-1 (P53675)	Coat protein for receptor mediated endocytosis of coated pits and vesicles (12)	10	69	77	121
COPA	Coatomer I-α (P53621)	Retrograde Golgi to ER vesicle transport (13)	4	22	6	25
COPB1	Coatomer I-β1 (P53618)	Retrograde Golgi to ER vesicle transport (13)	1	23	1	32
COPG	Coatomer- I γ (Q9Y678)	Retrograde Golgi to ER vesicle transport (13)	15	31	28	43
COPD	Coatomer- I δ (P48444)	Retrograde Golgi to ER vesicle transport (13)	8	12	12	13
Enzymatic function						
CAPN2	Calpain-2 (P17655)	Cell migration, invasion and survival, focal adhesion turnover, leading edge polarity (14)	2	18	6	19
FASN	Fatty acid synthase (P49327)	Fatty acid and lipid biosynthesis, upregulated in cancer, oncogenic function (15)	8	91	14	98
MAPK1	Extracellular signal regulated kinase-2 (ERK2) (P28482)	MAP kinase signaling, promotes proliferation, survival, oncogenesis (16)	0	7	0	7
PAK2	P21 (Rac/Cdc42) activated kinase 2 (Q13177)	Rac/Cdc42 linked protein serine/threonine kinase activity , cancer cell invasion (17)	0	7	17	16
PPP2R1A	Protein phosphatase 2 regulatory subunit A, alpha, PR65A (P30153)	HEAT repeat subunit of PP2A, PP2A scaffolding and assembly, substrate interactions (18)	2	7	3	12
RNH1	Ribonuclease/angiogenin inhibitor 1 (P13489)	Cytoplasmic RNase inhibitor, control of mRNA turnover (19)	0	12	0	20

Protein binding and recognition						
CCT5	Chaperone TCP1, subunit 5 (P48643)	Protein folding and recognition through chaperone containing TCP1 ring complex; biogenesis of actin, tubulin (20)	8	22	43	49
CSE1L	Exportin-2, Isoform 1 (P55060)	Nuclear export receptor for importin α *via* RanGTP; cancer cell cycle, cell invasion and metastasis (21,22)	0	7	0	7
KPNB1	Karyopherin (importin) β1 (Q14974)	Nuclear localization signal receptor, mediates cargo-importin α interactions with nuclear pores (23)	7	14	36	36
PCBP1	Heterogeneous nuclear riboprotein E1 (Q15365)	RNA recognition and binding, translational coactivator, mRNA stability (24)	4	10	36	33

C. SUPPLEMENTAL MOVIES

Movie S1. The WRAMP structure forms dynamically and is dependent on Rho kinase, related to Figure 1.

Movie S2. Coordinated recruitment of MCAM and endoplasmic reticulum to the WRAMP structure, related to Figure 6.

Movie S3. Coordination between the WRAMP structure and Ca^{2+} release, related to Figure 7.

Movie S1. The WRAMP structure forms dynamically and is dependent on Rho kinase, related to Figure 1. This movie has three sections:

(1) **The WRAMP structure forms dynamically, related to Fig. 1A.** WM239A cell cultured on plastic plates, showing dynamic polarization of MCAM-RFP and GFP-myosin IIb heavy chain, followed temporally by membrane retraction and condensation of the GFP-myosin IIb into a punctate structure.

(2) **The WRAMP structure in hydrogel culture, related to Fig. 1B.** WM239A cells expressing MCAM-GFP are embedded into a hydrogel matrix, photopolymerized with RGD and MMP–degradable crosslinking peptides. Cell movement through the matrix requires MMP-dependent peptide proteolysis for 3D cell invasion, due to a hydrogel mesh size of ~50 nm (Schwartz et al., 2010). MCAM-GFP appears stably localized at the end of cells opposite to the direction of invasion, consistent with localization to the cell posterior.

(3) **Dependence of the WRAMP structure on Rho kinase, related to Fig. 1E.** WM239A cells expressing MCAM-GFP were embedded into hydrogel matrix photopolymerized with RGD and MMP peptides, and incubated in the presence of the Rho kinase inhibitor, Y27632 (10 μM), WM239A cells appear to lose polarity, and MCAM-GFP expression indicates failure to form stable WRAMP structures, seen by spatial splitting of signal and lack of coordinated movement within the cell.

Movie S2. Coordinated recruitment of MCAM and endoplasmic reticulum to the WRAMP structure, related to Figure 6D. WM239A cell co-expressing MCAM-GFP and ER-RFP shows coordinated movement of both WRAMP and the ER marker to the trailing edge, followed by membrane retraction.

Movie S3. Coordination between the WRAMP structure and Ca^{2+} release, related to Figure 7. This movie has four sections:

(1) **Calcium mobilization follows formation of the WRAMP structure, related to Fig. 7B.** WM239A cells were transfected to co-express the (Left) Cameleon calcium FRET biosensor and (Right) the ER marker, ER-RFP, and treated with Wnt5a. Formation of a WRAMP structure, monitored by ER-RFP, is followed by an increase in FRET signal (blue to red) which is in turn followed by membrane retraction.

(2) **Calcium channel inhibitors SKF-96365 + ryanodine block membrane retraction, related to Fig. 7C.** MCAM-GFP expressing cells were pretreated with 5 µM SKF-96365 + ryanodine for 1 h and then treated with 150 ng/mL Wnt5a. MCAM-GFP continues to move asymmetrically while membrane retraction is blocked.

(3) **IP_3/TRP channels are needed for WRAMP-associated membrane retraction, related to Fig. 7C.** WM239A cells expressing MCAM-GFP were treated with Wnt5a, and at the moment of WRAMP structure formation (7 min) the IP_3/TRP channel inhibitor, 2-APB, was added to a final concentration of 2.5 µM. The WRAMP structure diassembled minutes following 2-APB addition, and membrane retraction was suppressed. When the media was replaced with fresh RPMI + 150 ng/mL Wnt5a in absence of 2-APB (24 min), the WRAMP structure was able to reassemble (30 min).

(4) **Calpain inhibitor-III blocks membrane retraction at the WRAMP structure, related to Fig. 7C.** Live imaging of MCAM-GFP expressing cells pretreated with 15 µM calpain inhibitor-III for 1 hour and then treated with 150 ng/mL Wnt5a. MCAM-GFP continues to localize asymmetrically while membrane retraction is blocked.

D. SUPPLEMENTAL EXPERIMENTAL PROCEDURES

Materials. Antibodies used were mouse anti-MCAM, rabbit anti-EEA1 (Santa Cruz Biotechnology), mouse anti- IQGAP1 (Invitrogen), mouse anti-clathrin (BD Transduction), anti-COP-Iβ and anti-GFP (Abcam), rabbit anti-myosin IIb and anti-58kDa Golgi protein (Sigma). Plasmids expressing MCAM-GFP and IQGAP1-RFP, ER-RFP (from Eric Snapp, Albert Einstein Univ.), myosin II heavy chain-RFP (from Robert Adelstein, NIH), and the Cameleon FRET biosensor (from Roger Tsien, UC San Diego) were described (Witze et al., 2008; Jeong et al., 2006; Snapp et al., 2006; Wei & Adelstein, 2000; Miyawaki et al., 1999).

Cell culture and handling. WM239A cells were maintained at or below 75% confluency, in RPMI + 10% FBS. For DNA transfection, cells were trypsinized, resuspended in RPMI + 10% FBS, and washed once and then resuspended in OptiMEM. Typically, 100 µL of transfection complex (1 µg DNA, 10 µL Fugene, 100 µL OptiMEM) was added to 6 well plates (8 x10^4 cells, 2 mL) and incubated overnight at 37^{o}C, then the media was replaced with RPMI+10% FBS. For drug treatment, cells were preincubated with inhibitor (2.5 μM) or DMSO for 1 h at 37^{o}C, and media was replaced with RPMI+250 ng/mL Wnt5a for 30 min at 37^{o}C. For experiments with 2-APB, cells incubated with Wnt5a were monitored by live cell imaging on the heated stage and inhibitor was added at the moment of WRAMP structure formation to a final concentration of 2.5 μM.

COP-Iβ, IQGAP1 and Dvl2 knockdowns were performed using siGenome SMARTpool or individual siRNA duplex oligonucleotides (Dharmacon). Cells were trypsinized and resuspended in RPMI+10% FBS, washed once, and resuspended in OptiMEM (Invitrogen), and 2 mL transfection mixture (50 pmol siRNA + 6 µL DMRIE-C, Invitrogen in OptiMEM) was added to 1 mL (5 x10^5) cells. Cells were then incubated on 6 cm plates at 37^{o}C for 5 h before replacing the media with RPMI+10% FBS.

For immunoprecipitation, cells were treated with or without Wnt5a for 30 min, then harvested in 50 mM Tris pH 8.0, 100 mM NaCl, 15 mM $MgCl_2$, 10 μg/mL leupeptin, 10 μg/mL aprotinin, 20 μg/mL pepstatin A). After centrifugation (15,000 rpm, 15 min, 4^{o}C), supernatants were incubated with anti-GFP or anti-COP Iβ antibody for 1 h, 4^{o}C followed by addition of protein A Sepharose, and proteins in the pellets were monitored by Western blotting.

For 3D experiments, cells were cultured in synthetic hydrogels based on a radical-mediated thiol-ene photopolymerization as described (Fairbanks et al., 2009; Schwartz et al., 2010). Briefly, 4-arm 20,000 MW poly(ethylene glycol)-norbornene (PEG-norbornene) was synthesized by coupling 4-arm PEG (JenKem USA) with norbornene acid (Sigma). Peptides were synthesized using solid Rink-amide resin using Fmoc chemistry on an Applied Biosystems 433A peptide synthesizer. Crosslinking was achieved using a peptide (KKCG**GPQG↓IWGQ**GCKK) based on a matrix metalloproteinase (MMP)-degradable amino acid sequence (shown in bold, cleavage site shown with arrow) found in collagen (Netzel-Arnett et al., 1991; Nagase & Fields, 1996) and incorporating cysteine on each end to faciliate crosslinking *via* reaction with the tetrafunctional PEG-norbornene macromolecules. Cell adhesion was promoted using peptides with the fibronectin sequence, C**RGD**S (Ruoslahti & Pierschbacher, 1987), containing terminal Cys pendant adhesion sites. A non-bioactive scrambled peptide was used for control experiments ("0 RGD"). Cells (300,000 cells/mL) were seeded in 3% (w/w) (PEG-norbornene + MMP-degradable crosslinking peptide) hydrogel disks (30 μL) with 1 mM CRGDS and swollen overnight in RPMI+10%FBS. After 24 h, live cell images were collected every 30 min for up to 36 h using a Nikon TE2000E automated microscope. Immunostaining was performed after 48 h using extended fixing (30 min), permeabilization (30 min), blocking (2 h), and rinsing (15 min each) to allow for diffusion into the gel, and overnight incubation at 4°C with primary and secondary antibodies. In ROCK inhibition experiments, 10 μM Y27632 (Sigma) was added after overnight swelling, 2 h before imaging.

Organelle proteomics. WM239A cells were grown on 15 cm dishes (5.3×10^6 cells/plate) in the presence or absence of Wnt5a, harvested by washing 3X with PBS and scraping into lysis buffer (10 mM Tris, pH 8, 1.5 mM $MgCl_2$, 10 mM KCl), and disrupted by passage through a 25G 3-5/8 inch needle. Nuclei were removed by centrifugation (800 g, 10 min, 4°C), and 2.5 mL supernatant was mixed with 1.35 mL 50% iodixanol to a final concentration of 17.5%, and transferred to a quick-seal centrifuge tube. A 700 μL cushion of 20% iodixanol was layered on the bottom and then overlaid with 700 μL 0.25 M sucrose in lysis buffer. Samples were ultracentrifuged without braking (Beckman L8-M, 350,000 g, 2 h), the tube bottoms were punctured, and 150 μL fractions collected. 150 μL lysis buffer was added to each fraction, followed by ultracentrifugation (TLA 100.3, 60,000 rpm, 20 min). Pellets were washed with 1 mL lysis buffer, centrifuged, resuspended with 0.1% Rapigest in 50 mM ammonium bicarbonate, and boiled for 10 min. Proteins were reduced, alkylated, and digested with 3 aliquots of 25 ng trypsin (Promega) each for 1 h at 37°C. Rapigest was then cleaved by adding 0.25 μL

trifluoroacetic acid and incubating for 45 min, 37°C, followed by centrifugation and removal of the bottom layer. The top (aqueous) layer containing peptides was stored at -80°C.

LC-MS/MS was carried out using a Thermo LTQ-Orbitrap mass spectrometer interfaced with a Waters nanoAcquity UPLC, and BEH C18 reversed phase column (25 cm x 75 μm i.d, 1.7 μm, 100Å, Waters). Peptide mixtures (5 μL, 2 μg) were loaded and separated by a linear gradient from 95% Buffer A (0.1% formic acid) to 40% Buffer B (0.1% formic acid, 80% CH_3CN) over 120 min at 300 nL/min. For each MS scan, the 10 most intense ions were targeted for MS/MS with dynamic exclusion 30 s, 1 Da exclusion width, and repeat count = 1, enabling monoisotopic precursor and charge selection settings, and excluding ions with charge state +1 or unassigned. The maximum injection time for Orbitrap parent scans was 500 ms, allowing 1 μscan and AGC $1x10^6$. The maximal injection time for the LTQ MS/MS was 250 ms, with 1 μscan and AGC $1x10^4$. The normalized collision energy was 35% with activation Q=0.25 for 30 ms.

Light and electron microscopy. For indirect immunofluorescence, cells were seeded on glass coverslips (500,000 cells) and grown for 24 h, washed once with 1 mL PBS, and incubated overnight in 1 mL RPMI without FBS. The media was removed, fresh RPMI without FBS containing 150 ng/mL Wnt5a was added, and cells incubated at 37^{o}C for 30 min. Cells were fixed in 4% formalin for 5 min at room temperature, permeabilized with 0.1% Triton X-100 in PBS, blocked with 5% BSA, 0.1% Tween/Tris-buffered saline and incubated with specified antibodies (1:200 dilution) followed by AlexaFluor-488 or -546 donkey anti-mouse or anti-rabbit secondary antibody (Invitrogen). Images were collected on a Olympus IX81 inverted microscope and analyzed with Slidebook software.

Live cell imaging was performed in an environmental chamber mounted on the Olympus microscope. Cells were serum-starved overnight, washed 1X with Hanks' Balanced Salt Solution (HBSS) and incubated in HBSS with 25 mM Hepes, pH 7.4. The stage temperature was set to 35^{o}C and images were collected every 30-60 s on GFP and RFP channels. Live imaging of the Cameleon FRET sensor was performed on a Nikon Eclipse TE2000-S inverted microscope and images were acquired with a CoolSNAP ES digital camera (Photometrics) and analyzed with MetaMorph software. The minimum ratio under Ca^{2+}-free conditions (R_{min}) was determined by incubating cells with 5 μM ionomycin, 3 mM EGTA, in Ca^{2+} free HHBSS, while the maximum ratio were measured with 5 μM ionomycin,10 mM $CaCl_2$. The ratio values were then converted to Ca^{2+} concentrations using the equation:

$[Ca^{2+}] = \{K'_d{}^n \times (R - R_{min})/(R - R_{max})\}^{1/n}$ $K'_d = 0.76$ μM, $n = 0.74$

For electron microscopy, cells were prepared as described (McDonald, 1984) with modifications. Samples were fixed for 30 min in 50 mM sodium cacodylate, 2% glutaraldehyde, rinsed in the same buffer, and post-fixed for 5 min with 0.5% osmium tetroxide, 0.8% $K_3Fe(CN)_6$. After rinsing, cells were stained for 1 min in 0.15% tannic acid, rinsed with water, dehydrated in acetone, and embedded in Epon Araldite resin. Cells were imaged with a Tecnai F-30 electron microscope (FEI Co., Einhoven, NL), using a Gatan CCD camera to record serial tilts from ±60° in increments of 1° using image acquisition software Serial EM (Mastronarde, 2005). Each section was imaged in 2 tilt series around orthogonal axes and then assembled into a single reconstruction using the IMOD software (Mastronarde, 1997). Tomographic reconstructions were modeled by manual contour tracing using IMOD (Kremer et al., 1996).

Supplemental References

1. Kim, H. and McCulloch, C.A. (2011) Filamin A mediates interactions between cytoskeletal proteins that control cell adhesion. *FEBS Lett.* 585:18-22.
2. Silacci, P., Mazzolai, L., Gauci, C., Stergiopulos, N., Yin, H.L., and Hayoz, D. (2004) Gelsolin superfamily proteins: key regulators of cellular functions. *Cell Mol Life Sci.* 61:2614-2623.
3. White, C.D., Brown, M.D., and Sacks, D.B. (2009) IQGAPs in cancer: a family of scaffold proteins underlying tumorigenesis. *FEBS Lett.* 583:1817-1824.
4. Even-Ram, S. and Yamada, K.M. (2007) Of mice and men: Relevance of cellular and molecular characterizations of myosin IIA to MYH9-related human disease. *Cell Adh Migr.* 1:152-155.
5. McConnell, R.E. and Tyska, M.J. (2010) Leveraging the membrane - cytoskeleton interface with myosin-1. *Trends Cell Biol.* 20:418-426.
6. Roberts, G.C. and Critchley, D.R. (2009) Structural and biophysical properties of the integrin-associated cytoskeletal protein talin. *Biophys Rev.* 1:61-69.
7. Akhmanova, A. and Hammer, J.A. (2010) Linking molecular motors to membrane cargo. *Curr Opin Cell Biol.* 22:479-487.
8. Yamada, M., Toba, S., Takitoh, T., Yoshida, Y., Mori, D., Nakamura, T., Iwane, A.H., Yanagida, T., Imai, H., Yu-Lee, L.Y., Schroer, T., Wynshaw-Boris, A. and Hirotsune, S. (2010) mNUDC is required for plus-end-directed transport of cytoplasmic dynein and dynactins by kinesin-1. *EMBO J.* 29:517-531.
9. Tischfield, M.A. and Engle, E.C. (2010) Distinct alpha- and beta-tubulin isotypes are required for the positioning, differentiation and survival of neurons: new support for the 'multi-tubulin' hypothesis. *Biosci Rep.* 30:319-330.
10. Malinin, N.L., Plow, E.F., and Byzova, T.V. (2010) Kindlins in FERM adhesion. *Blood* 115:4011-4017
11. Old, W.M., Shabb, J.S., Houel, S., Wang, H., Couts, K.H., Yen, C-Y., Litman, E.S., Croy, C.H, Meyer-Arendt, K., Miranda, J.G., Brown, R.A., Witze, E.S., Schweppe, R.E., Resing, K.A., and Ahn, N.G. (2009) Functional proteomics identifies targets of phosphorylation by B-Raf signaling in melanoma. *Molecular Cell,* 34:115-131.
12. McPherson, P.S. (2010) Proteomic analysis of clathrin-coated vesicles. *Proteomics* 10:4025-4039.
13. Bethune, J., Wieland, F., Moelleken, J. (2006) COPI-mediated transport. *J. Membr. Biol.* 211:65-79.
14. Storr, S.J., Carragher, N.O., Frame, M.C., Parr, T. and Martin, S.G. (2011) The calpain system and cancer. *Nat Rev Cancer. 1*1:364-374.
15. Liu, H., Liu, J.Y., Wu, X. and Zhang, J.T. (2010) Biochemistry, molecular biology, and pharmacology of fatty acid synthase, an emerging therapeutic target and diagnosis/prognosis marker. *Int J Biochem Mol Biol.* 1:69-89.
16. Shaul, Y.D. and Seger, R. (2007) The MEK/ERK cascade: from signaling specificity to diverse functions. *Biochim Biophys Acta.* 1773:1213-1226.
17. Whale, A., Hashim, F.N., Fram, S., Jones, G.E. and Wells, C.M. (2011) Signalling to cancer cell invasion through PAK family kinases. *Front Biosci.* 16:849-864.
18. Zolnierowicz, S. (2000) Type 2A protein phosphatase, the complex regulator of numerous signaling pathways. *Biochem Pharmacol.* 60:1225-1235.
19. Dickson, K.A., Haigis, M.C. and Raines, R.T. (2005) Ribonuclease inhibitor: structure and function. *Prog Nucleic Acid Res Mol Biol.* 80:349-374.
20. Brackley, K.I. and Grantham, J. (2009) Activities of the chaperonin containing TCP-1 (CCT): implications for cell cycle progression and cytoskeletal organisation. *Cell Stress Chaperones* 14:23-31.
21. Tai, C.J., Hsu, C.H., Shen, S.C., Lee, W.R. and Jiang, M.C. (2010) Cellular apoptosis susceptibility (CSE1L/CAS) protein in cancer metastasis and chemotherapeutic drug-induced apoptosis. *J Exp Clin Cancer Res.* 29:110.
22. Kutay, U., Bischoff, F.R., Kostka, S., Kraft, R. and Gorlich, D. (1997) Export of importin alpha from the nucleus is mediated by a specific nuclear transport factor. *Cell* 90:1061-1071
23. Xu, D., Farmer, A. and Chook, Y.M. (2010) Recognition of nuclear targeting signals by Karyopherin-β proteins. *Curr Opin Struct Biol.* 20:782-790.
24. Makeyev, A.V. and Liebhaber, S.A. (2002) The poly(C)-binding proteins: a multiplicity of functions and a search for mechanisms. *RNA.* 8:265-278.